Supplementary Information

The Structural Properties and Photoelectrocatalytic Response of Mn-doped Hematite Photoanodes Prepared via a Modified Electrodeposition Approach

Pannan I. Kyesmen[12*], Joseph Simfukwe[3], Peverga R. Jubu[2], Adedapo O. Adeola[4], and Mmantsae Diale[1*]

Pannan I. Kyesmen, Mmantsae Diale
University of Pretoria, Department of Physics, Private Bag X20, Hatfield 0028, South Africa
Email addresses: pannan.kyesmen@tuks.co.za; mmantsae.diale@up.ac.za

Pannan I. Kyesmen, Peverga R. Jubu
Department of Physics, Joseph Sarwuan Tarka University Makurdi (formerly, University of Agriculture Makurudi)

Joseph Simfukwe
Copperbelt University, Physics Department, Riverside, Kitwe 10101, Zambia

Adedapo O. Adeola
Department of Chemistry and Biochemistry and the Centre for NanoScience Research, Concordia University, Canada, Montréal, QC, H4V 1R6.

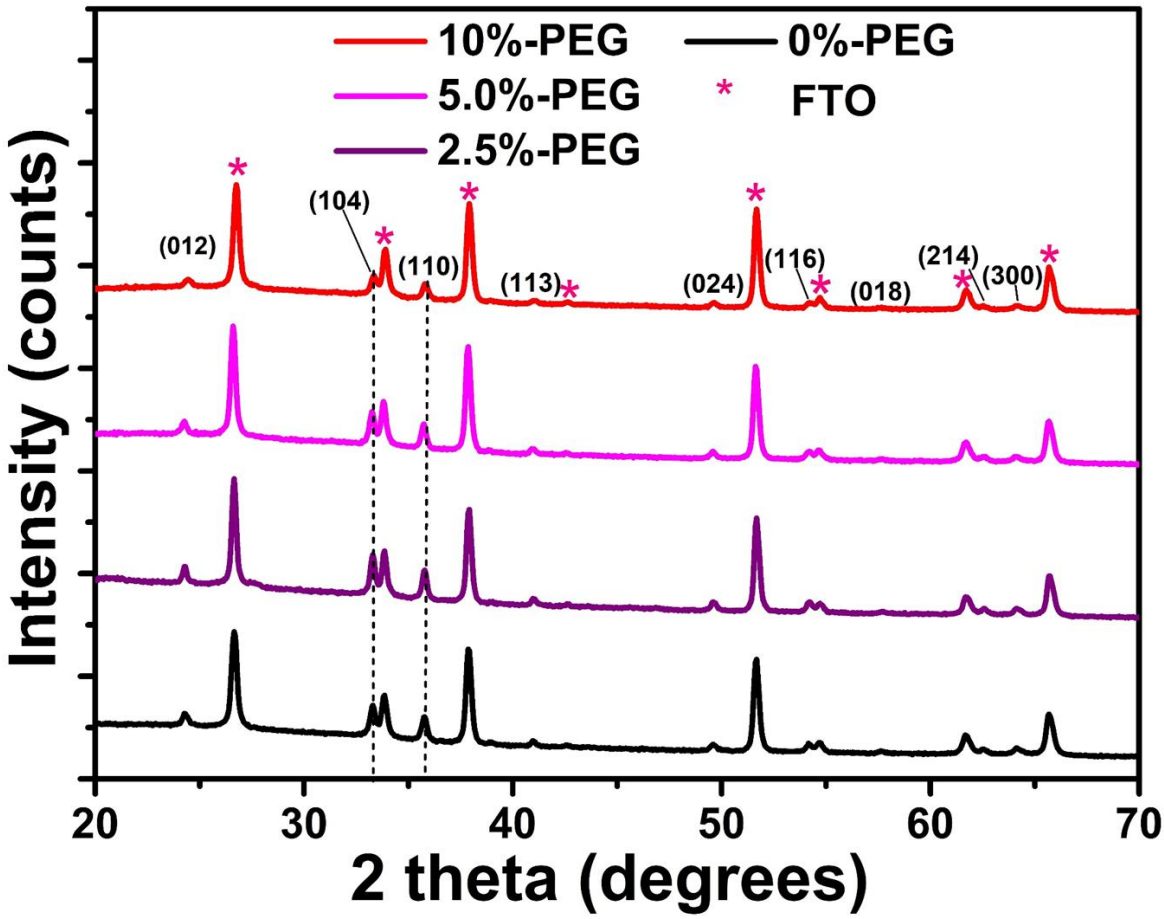

Fig. S1. XRD patterns of pristine electrodeposited α-Fe_2O_3 films prepared using electrolytes modified various percentages of PEG 400.

Table S1. XRD analysis preventing the FWHM, crystal size, microstrain, and dislocation density undoped and dope hematite films.

Sample	Bragg angle (2θ)	FWHM (degrees)	Crystal size (nm)	Strain ε x 10^{-3}	Dislocation density ɖ x 10^{15} Lin/m^2
0%-PEG	35.764	0.295	28.3	3.99	1.25
2.5%-PEG	35.772	0.277	30.2	3.75	1.10
5.0%-PEG	35.734	0.284	29.4	3.84	1.16
10%-PEG	35.811	0.302	27.6	4.09	1.31
1%-Mn	35.843	0.313	26.7	4.26	1.40
3%-Mn	35.585	0.352	23.7	4.79	1.78
6%-Mn	35.595	0.366	22.8	4.98	1.92
10%-Mn	35.571	0.374	22.3	5.09	2.01

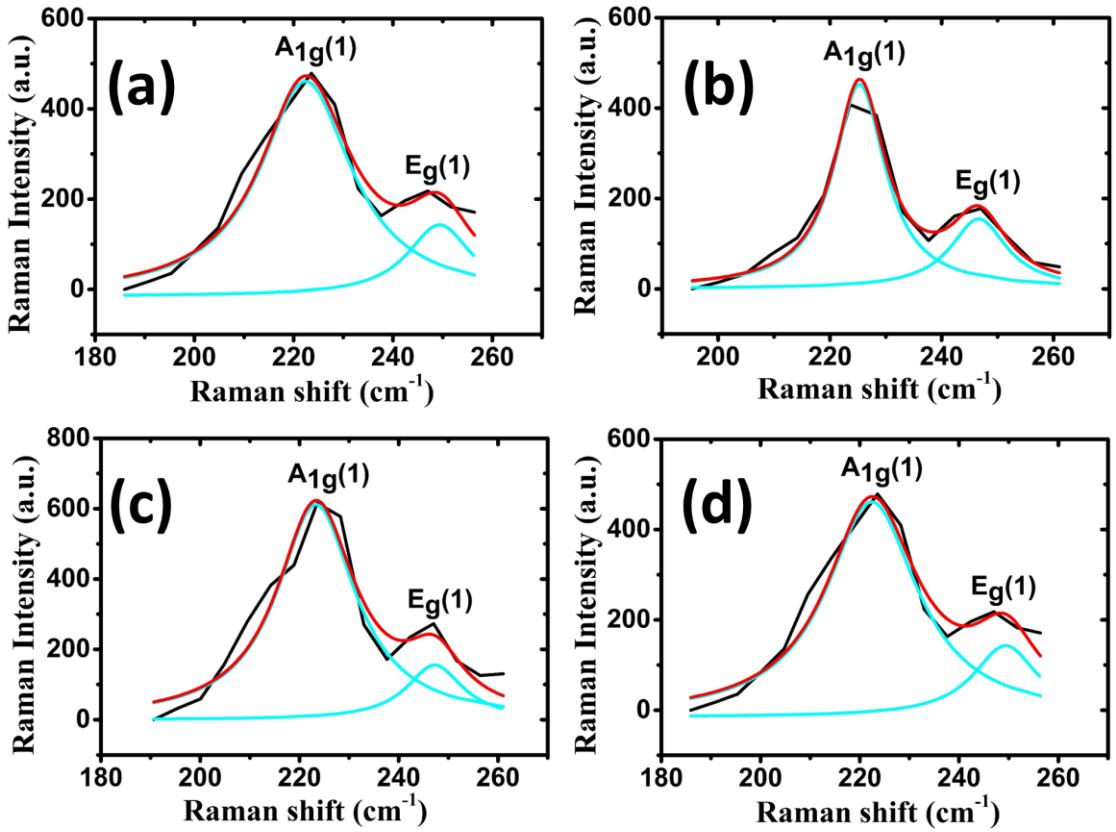

Fig. S2. Lorentzian fitting and deconvolution curves for the first two phonon modes of the Raman spectra of (a) 0%-PEG, (b) 2.5%-PEG, (c) 5%-PEG, and (d) 10%-PEG pristine α-Fe_2O_3 samples.

Table S2. The deconvolution results of the first two vibrational modes of the Raman spectra of the pristine and Mn-doped α-Fe_2O_3 samples.

Sample	Peak position, υ (cm^{-1})		FWHM (cm-1)	
	$A1_g(1)$	$E_g(1)$	$A1_g(1)$	$E_g(1)$
0%-PEG	217.9	224.7	20.81	23.39
2.5%-PEG	225.3	246.4	11.21	12.56
5.0%-PEG	223.6	246.6	19.19	13.85
10%-PEG	223.2	248.8	22.42	15/84
1%-Mn	222.8	243.3	13.04	12.85
3%-Mn	220.5	243.1	14.87	13.82
6%-Mn	221.3	243.5	12.47	13.22
10%-Mn	221.6	244	16.97	14.75

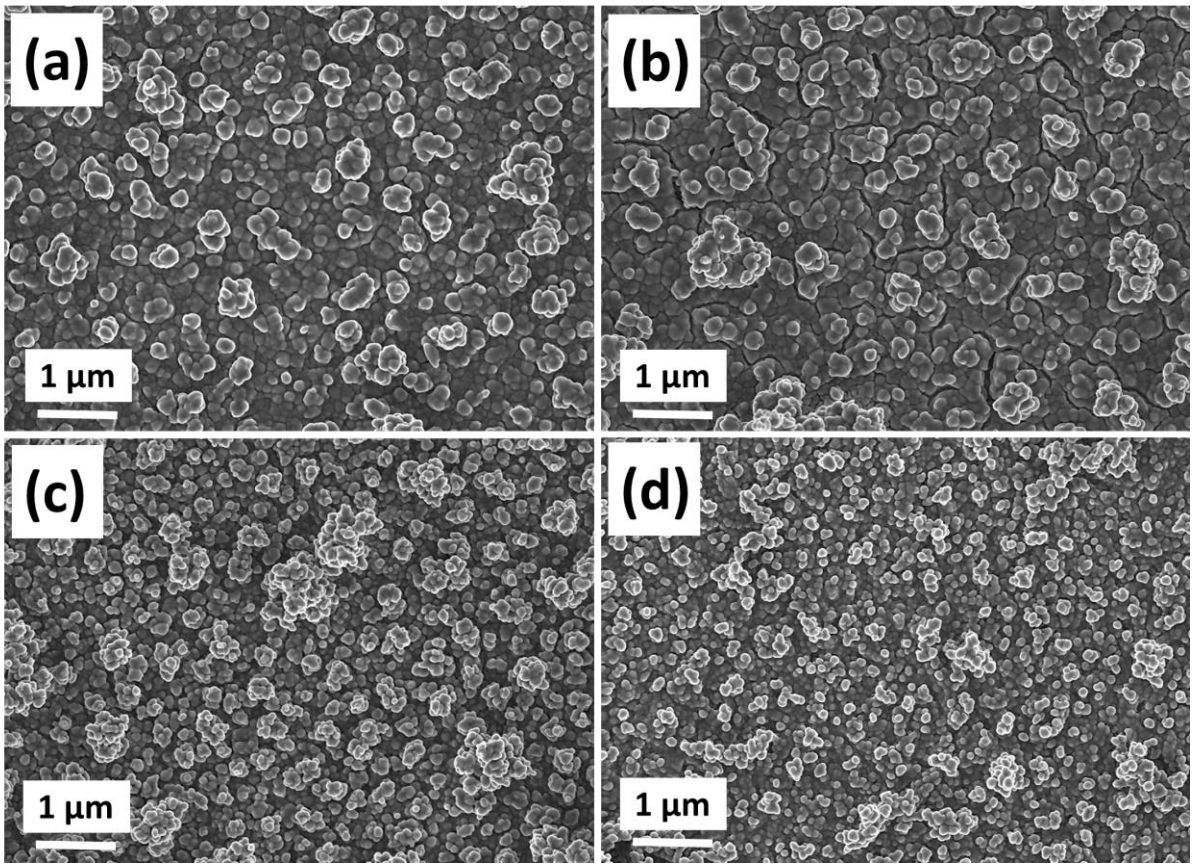

Fig. S3. The surface images of (a) 1%-Mn, (b) 3%-Mn, (c) 6%-Mn, and (d) 10%-Mn doped α-Fe_2O_3 samples.

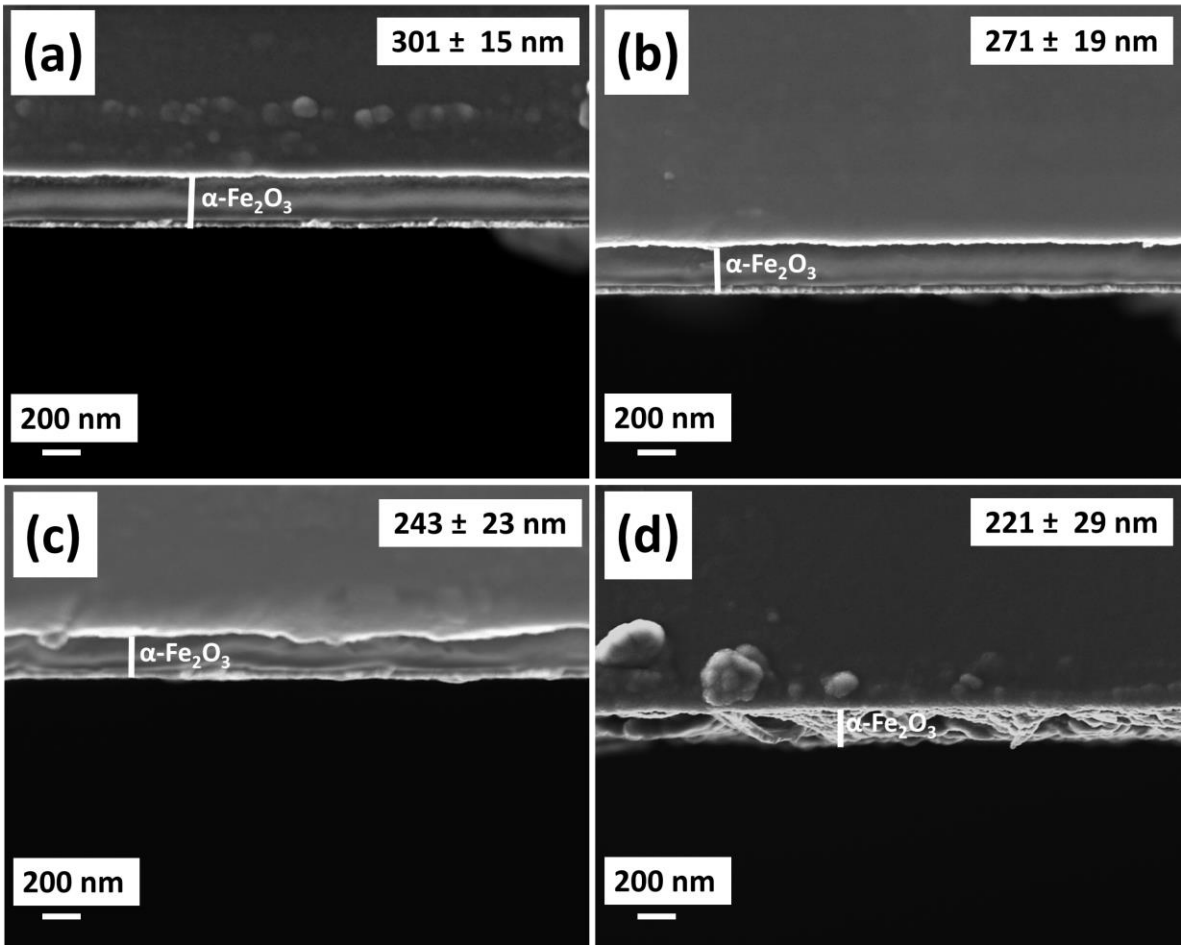

Fig. S4. The surface micrographs of pristine hematite films for (a) 0%-PEG, (b) 2.5%-PEG, (c) 5.0%-PEG, and (d) 10%-PEG samples.

The TAUC formula used to obtain approximate bandgap values of the pristine and Mn-doped α-Fe_2O_3 films is given in equation S1:

$$\alpha h\nu = A\left(h\nu - E_g\right)^n \quad \text{(S1)}$$

where h represents the Planck constant, ν stands for the frequency of light, A represents an arbitrary constant, E_g denotes the band gap and n is a constant which equals 2 for allowed indirect transitions and 1/2 for direct transitions (Li 2014). The indirect transitions that occur in α-Fe_2O_3 films are linked to the spin-forbidden Fe^{3+} 3d to 3d excitations while the direct transitions are due to charge transfer from O^{2-} 2p to Fe^{3+} 3d [1]. The graphs of $(\alpha h\nu)^{1/2}$ against $h\nu$ given in Fig. 7 (c) and (d) of the main manuscript for the undoped and Mn-doped samples respectively were plotted, and after extrapolating the linear portion of the curves, the intersect at ($h\nu$)-axis yielded the indirect band gap values of the films.

Table S3. Indirect bandgap values of undoped and doped hematite films.

Sample	Indirect Bandgap (eV)
0%-PEG	2.11
2.5%-PEG	2.06
5.0%-PEG	2.07
10%-PEG	2.02
1%-Mn-doped	2.05
3%-Mn-doped	2.00
6%-Mn-doped	1.99
10%-Mn-doped	2.04

Table S4. The bandgap values obtained from DFT calculations for three doped α-Fe_2O_3 systems

Doped α-Fe_2O_3 layer (L)	Band gap (eV)
Pristine Hematite	2.17
2.1% Mn-doped L2	2.18
4.2 % Mn-doped L2	2.19
4.2 % Mn-doped L2_3	2.08

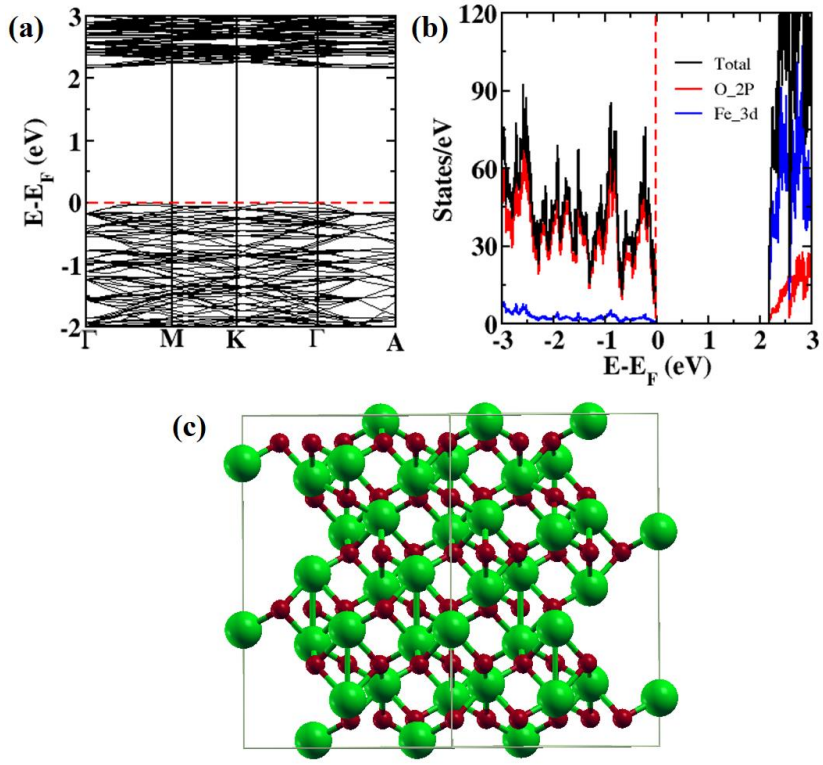

Fig. S5. The band structure and partial density of states (PDOS) of pristine hematite (a) and (b) respectively and a relaxed 2 x 2 hexagonal hematite structure (c). The Fermi level is set to zero. Color scheme: Green (large sphere) and red (small sphere) denote Fe and O atoms respectively.

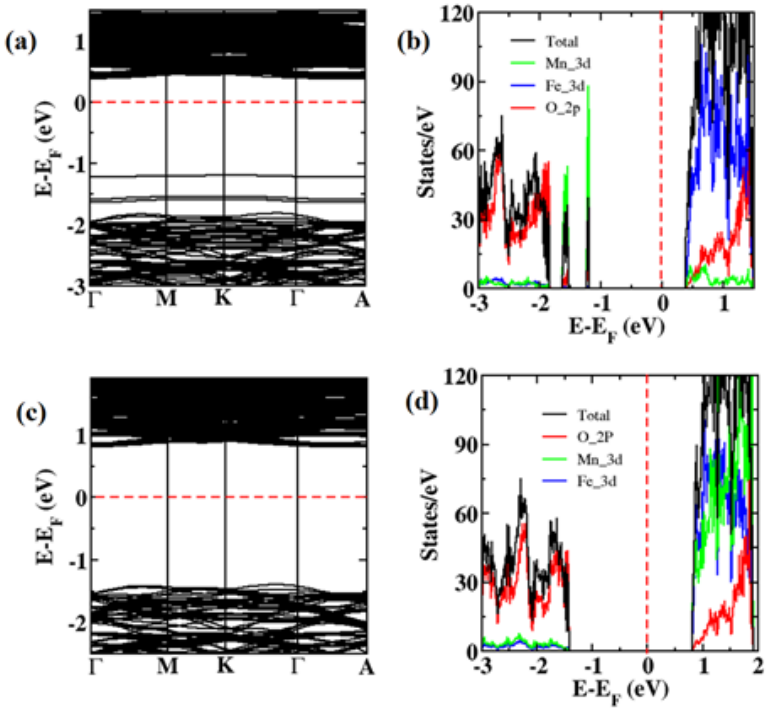

Fig. S6. The band structure and the partial density of states (PDOS) for 2.1 % Mn-doped layer 3 (a) and (b), 4.2 % Mn-doped layer 2 and 3 (c) and (d). The dashed line denotes the Fermi level of the doped hematite.

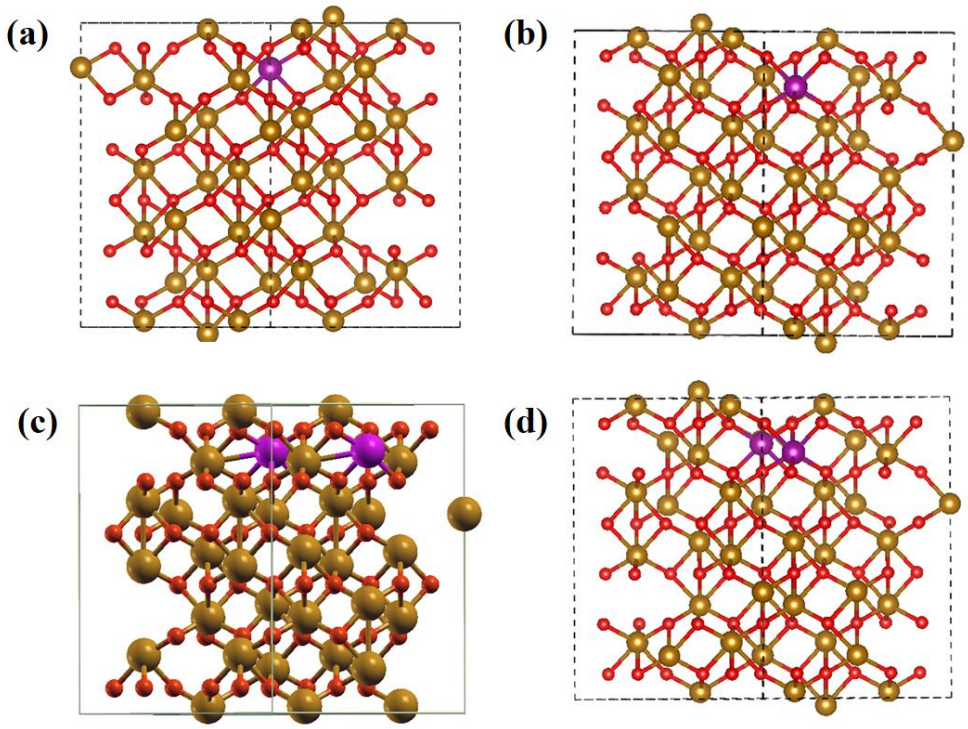

Fig. S7. The relaxed doped system (a) 2.1% Mn doped layer 2 (b) 2.1 % Mn doped layer 3 (c) 4.2 % Mn doped layer 2 and (d) 4.2 % doped layers 2 and 3.

Table S5. A comparison of the optimal photocurrent density obtained for Mn-doped hematite and the photocurrent enhancement achieved over the pristine samples with other reported values for the doped material where metallic dopants were used.

α-Fe_2O_3 dopant, Nanostructure, preparation method, and annealing temperature	**Optimal photocurrent density (J)**	**Photocurrent increase relative to the pristine films**	**Ref.**
Mn, Nanoparticles, Electrodeposition	0.32 mA/cm^2 at 1.5 V vs RHE, 1 M NaOH electrolyte, 1 sun	6.1-fold	This work
La, Nanotubes, Electrospinning, 500ºC	0.204 mA/cm2 at 1.6 V vs RHE, 1 M NaOH electrolyte, 1 sun	1.4-fold	[2]
Zr, Nanoparticles, Solvothermal, 700ºC	0.52 mA/cm2 at 1.5 V vs RHE, 1 M KOH electrolyte, 1 sun	4.0-fold	[3]
Sn, Nanorods, hydrothermal, 550ºC	>0.4 mA/cm2 at 1.5 V vs RHE and 3.0 mA/cm2 at 2.0 V vs RHE, 1 M NaOH electrolyte, 1 sun	Not given	[4]
La, Nanoparticles, Electrospinning, 500ºC	0.27 mA/cm2 at 1.6 V vs RHE, 1 M NaOH electrolyte, 1 sun	1.6-fold	[2]
Zn, Nanograins, pulsed laser deposition, 1200ºC	0.38 mA/cm^2 at 1.23 V vs RHE, 1 M NaOH electrolyte,	1.3-fold	[5]
Ti, Nanoworms, Liquid phase deposition, 850ºC	0.50 mA/cm^2 at 1.23 V vs RHE, 1 M KOH electrolyte, 1 sun	1.6-fold	[6]
Pt, Nanoparticles, Electrodeposition, 700ºC	0.56 mA/cm^2 at 1.4 V vs RHE, 1 M NaOH electrolyte, 1 sun	1.4-fold	[7]
Mg, Nanoparticles, Hydrothermal, 750ºC	1.04 mA/cm^2 at 1.23 V vs RHE, 1 M NaOH electrolyte, 1 sun	2.8-fold	[8]
Zr, Nanorods, Hydrothermal and magnetron sputtering, 800ºC	1.23 mA/cm^2 at 1.23 V vs RHE, 1 M NaOH electrolyte, 1 sun	1.9-fold	[9]
Ca, Nanorods, Hydrothermal, 800ºC	0.31 mA/cm^2 at 1.23 V vs RHE, 1 M NaOH electrolyte, 1 sun	2.0-fold	[10]

References

[1] F. L. Souza, K. P. Lopes, P. A. Nascente, E. R. Leite, *Sol. Energy Mater. Sol. Cells* **2009**, 93, 362.

[2] N. Li, S. Jayaraman, S. Y. Tee, P. S. Kumar, C. J. J. Lee, S. L. Liew, D. Chi, T. A. Hor, S. Ramakrishna, H.-K. Luo, *J. Mater. Chem. A* **2014**, 2, 19290.

[3] B. J. Rani, M. P. Kumar, G. Ravi, S. Ravichandran, R. K. Guduru, R. Yuvakkumar, *Appl. Surf. Sci.* **2019**, 471, 733.

[4] B. J. Rani, G. Ravi, R. Yuvakkumar, S. Ravichandran, F. Ameen, S. AlNadhary, *Renewable energy* **2019**, 133, 566.

[5] A. Kay, D. A. Grave, D. S. Ellis, H. Dotan, A. Rothschild, *ACS Energy Letters* **2016**, 1, 827.

[6] M. Rasouli, A. Yourdkhani, R. Poursalehi, *Mat. Sci. Semicond. Process* **2022**, 142, 106476.

[7] G. Rahman, O.-S. Joo, *Mater. Chem. Phys.* **2013**, 140, 316.

[8] Q. Du, Y. Guan, Q. Deng, S. Wang, Z. Li, H. He, S. Yan, *ACS Applied Nano Materials* **2023**, 6, 12459.

[9] H. Ma, J. B. Hwang, W. S. Chae, H. S. Chung, S. H. Choi, M. A. Mahadik, H. H. Lee, J. S. Jang, *Appl. Surf. Sci.* **2021**, 549, 149233.

[10] S. Wang, C. Meng, Y. Bai, Y. Wang, P. Liu, L. Pan, L. Zhang, Z. Yin, N. Tang, *ACS Applied Nano Materials* **2022**, 5, 6781.